Journal of Power Sources 206 (2012) 3–13

Contents lists available at SciVerse ScienceDirect

Journal of Power Sources

journal homepage: www.elsevier.com/locate/jpowsour

Review

Materials selection for bipolar plates for polymer electrolyte membrane fuel cells using the Ashby approach

Mara Cristina Lopes de Oliveira[a], Gerhard Ett[a], Renato Altobelli Antunes[b,*]

[a] Electrocell Ind. Com. Equip. Elet. LTDA, Technology, Entrepreneurship and Innovation Center (CIETEC), 05508-000 São Paulo, SP, Brazil
[b] Engineering, Modeling and Applied Social Sciences Center (CECS), Federal University of ABC (UFABC), 09210-170 Santo André, SP, Brazil

ARTICLE INFO

Article history:
Received 13 December 2011
Received in revised form 15 January 2012
Accepted 16 January 2012
Available online 8 February 2012

Keywords:
Bipolar plates
PEM fuel cells
Materials selection
Ashby charts

ABSTRACT

In this work the Ashby approach was used to select materials for bipolar plates for polymer electrolyte membrane (PEM) fuel cells. The procedure was based on the development of a trade-off strategy based on the evaluation of the corresponding Ashby charts. A detailed analysis of relevant performance attributes for different types of materials traditionally used as bipolar plates is given. The data used in the selection process were collected from the scientific literature and from datasheets of commercial products. In this regard, graphite–polymer composites and metals are thoroughly compared owing to their mechanical, electrical and corrosion properties. The results evidenced the suitability of the Ashby approach as a reliable method to assist the designer of bipolar plates in the complex task of selecting materials that allow for the best overall performance.

Contents

1. Introduction 3
2. The Ashby approach 4
3. The strategy for selecting bipolar plates 5
   3.1. Materials selection for polymer–graphite composite bipolar plates 6
   3.2. Materials selection for metallic bipolar plates 6
4. Results and discussion 6
   4.1. First screening 6
   4.2. Screening and ranking for polymer–graphite composites 7
   4.3. Screening and ranking for metallic bipolar plates 9
5. Conclusions 11
   Acknowledgements 12
   References 12

1. Introduction

Fuel cells have a remarkable potential as low emission power generation sources [1]. This characteristic has been extensively explored through different technologies. Solid oxide (SOFC) and polymer electrolyte membrane (PEM) fuel cells are the most promising types of fuel cells toward the standardization of a hydrogen economy policy worldwide [2,3]. PEM fuel cells have well-known commercial applications owing to their fast start-up and high energy efficiency [4,5]. Nevertheless, full scale commercialization is still incipient. In this context, durability and cost are two major issues [6]. Bipolar plates are strongly related to these issues [7,8]. They are vital components of PEM fuel cells due to their core functions in the system, being responsible for the water and thermal management, current collection and distribution of fuel and oxidant within the cell [9]. To perform such a central role, bipolar plates have to be carefully designed to achieve specific technical requirements related to mechanical, electrical, thermal and chemical properties [10]. Furthermore, an attractive compromise between performance and cost must be pursued. Cost is a major barrier to the commercialization of PEM fuel cells. Wang et al. gave an excellent overview of the current status of PEM fuel cell development [11]. They addressed critical inter-related issues such as cost, technologies and the need for

* Corresponding author. Tel.: +55 11 4996 8241; fax: +55 11 4996 8241.
E-mail address: renato.antunes@ufabc.edu.br (R.A. Antunes).

0378-7753/$ – see front matter © 2012 Elsevier B.V. All rights reserved.
doi:10.1016/j.jpowsour.2012.01.104

fundamental research in vital components such as membrane, gas diffusion layer, catalysts, gas flow channels and bipolar plates. The gas flow field design is closely related to the PEM fuel cell performance. It affects the pressure of the reactant gases along the channels and, therefore, their mass transport rate to and from the anode and cathode [12]. The optimization of the flow field design enhances the performance of bipolar plates. The importance of the transport phenomena along the gas flow channels to the performance of PEM fuel cells has been evidenced by several authors [13–16]. In addition to the transport of the reactant gases through gas flow channels, bipolar plates also act as cooling plates, being responsible for the transport of water or air to the heat management of the PEM fuel cell [17]. Cooling channels design is also of prime importance to the performance of bipolar plates [18,19]. New knowledge has been brought to this area by the development of suitable mathematical models that successfully explain the fluid and electron transport phenomena in PEM fuel cells [20–23]. These aspects and the final output voltage of the fuel cell are coupled to the properties of the materials employed to fabricate bipolar plates.

A first insight into this complex scenario evidences that the development of bipolar plates for PEM fuel cells is restricted by the intrinsic limitations of the materials employed in their manufacturing, regarding both performance and cost. Pure graphite emerged as the standard material for this application owing to its well-known high electrical conductivity and corrosion resistance. Nevertheless, the intrinsic brittleness of pure graphite is a serious obstacle to its widespread use, especially if one considers PEM fuel cells for transportation uses [24]. Graphite–polymer composites have been tentatively developed to circumvent the limitations of pure graphite plates, providing better mechanical stability to the final product. Several different polymeric matrices have been employed as binders to the conductive graphite particles, comprising both thermoplastic and thermosetting resins [25]. As the organic matrix is added to the graphite-based plate the consequent increase of mechanical strength is inevitably accompanied by a reduction of electrical conductivity. In this regard, a careful balance between these two properties must be ascertained. A common approach to improve the electrical performance of polymer–graphite composite bipolar plates is to add minor quantities of highly conductive carbon-based fillers such as carbon black, carbon nanotubes and carbon fibers [26,27]. As a consequence, many novel materials can be obtained by the specific mixing of proper fillers. In spite of some excellent results encountered in the literature regarding the electrical conductivity of polymer–graphite composite bipolar plates [28–30], metallic materials are more conductive and tougher [31]. Yet, engineering metallic alloys are readily available for mass production at a relatively low cost, without the need for laborious manufacturing steps as is frequently the case of carbon-based composite bipolar plates. The major drawback of metallic bipolar plates is the susceptibility to corrosion in the typical acid and humid environment of PEM fuel cells [32]. Corrosion resistance is, therefore, a key property in this case. Surface modification methods are profusely employed to overcome this limitation [33]. Many different techniques of producing protective coatings may give rise to an impressive multiplicity of materials with specific surface properties. Some examples are nitriding, ion implantation, physical vapor deposition, chemical vapor deposition and electrodeposition [34–38]. The same coating deposited through different techniques can yield distinct performances regarding both electrical conductivity and corrosion resistance [39,40]. Moreover, the same coating deposited by means of the same method but through different processing parameters can also yield distinct performances due to the formation of specific structure-related defects [41]. The list of alternatives to the manufacturing of bipolar plates is thereby further increased.

From the above considerations it is clear that the bipolar plate designer has to deal with a broad set of materials during the selection of the best candidates to the final product. The expertise of this critical step determines the identification of the most proper choices and delineates the pathways into a successful design. This challenging assignment is entangled by the huge amount of engineering materials available today. Ashby [42] estimated this number as more than 120,000. At one hand, such impressive list unfolds many possibilities, but on the other, it also hampers the task of identifying the best candidates straightforwardly. Moreover, the material attributes for bipolar plates span multiple properties and the designer has to decide whether a property is more important than other for a specific application. There is an evident trend in the literature toward considering electrical conductivity and mechanical strength as the most important attributes for polymer–graphite composite bipolar plates. For metallic-based components the corrosion resistance and the interfacial contact resistance are more frequently addressed. However, there is no apparent consensus on the relative importance of these attributes or if they stand only to a specific family of engineering materials. For instance, some reports indicate that carbon-based bipolar plates interact with the PEM fuel cell environment and deteriorates with time [43,44]. Hence, corrosion resistance would not be concerned only with metallic bipolar plates. This puzzling sketch constitutes an exciting materials selection problem that has been hardly discussed in the literature. An exception is the report by Shanian and Savadogo [45]. These authors used a multiple attribute decision making approach to select the best candidates for the manufacturing of metallic bipolar plates. Rao [46] complemented this view by introducing a compromise ranking method for metallic bipolar plates. Many reports are devoted to establish reliable and logical materials selection methods for a variety of industrial applications [47–51]. Jahan et al. [52] gave an excellent overview of different methodologies of materials screening and selection.

In spite of the valuable contributions by Shanian and Savadogo [45] and Rao [46] to the development of rational methods of materials selection for metallic bipolar plates, there are still many aspects to be unraveled. The influence of surface treatments, for instance, was not taken into account in these investigations. In the same way, composite bipolar plates have never been systematically assessed owing to materials selection methods. The aim of this work is to fill this gap. The Ashby approach was chosen as the methodology to meet this goal. This selection strategy was developed by Prof. Ashby at the Cambridge University. It is based on the use of the CES (Cambridge Engineering System) software to construct materials property charts. Next section describes the relevant aspects of this methodology supporting the arguments discussed throughout this text. A detailed view of this strategy is found in [42].

2. The Ashby approach

The selection strategy developed by Ashby is design-driven. In this respect, it starts by identifying the desired materials properties profile. Next, this profile is compared with real engineering materials to highlight the best match. The identification of the attributes to a given application is based on a translation step which comprises four different actions: (i) to express the function(s) that the material will perform; (ii) to label the constraint(s) for the application; (iii) to define the objective(s); (iv) to recognize which variables the designer is free to decide. With this information, next step is to screen all the available materials using the constraints. By doing so, the number of candidates is significantly reduced in comparison with the initial universe of options. Then, the remaining alternatives are ranked using the objective(s). Finally, the designer should search for supporting information regarding, for instance, the history of the top-ranked candidates owing to the application under

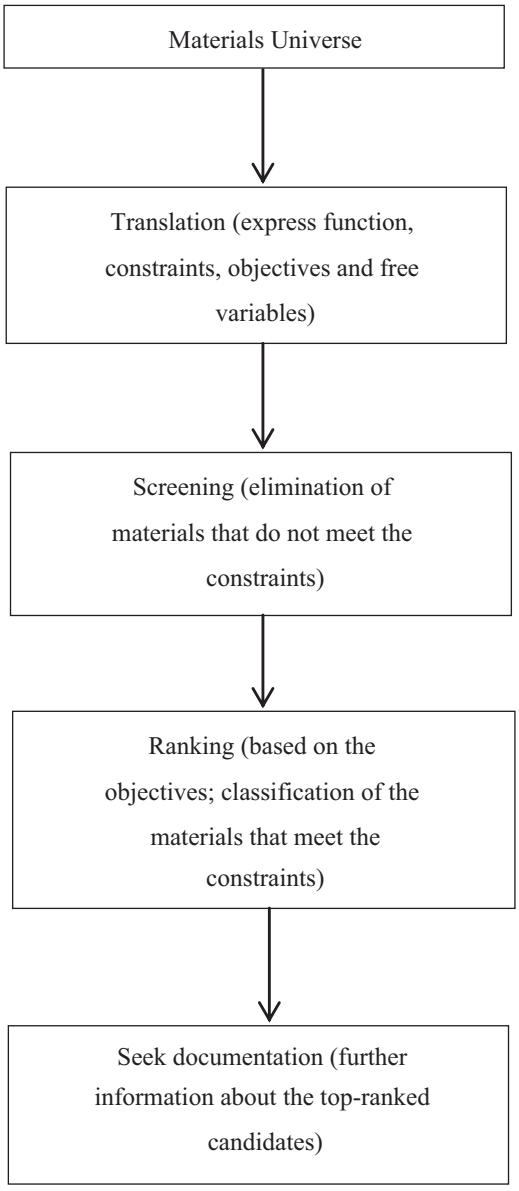

Fig. 1. Illustration of the different steps involved in the materials selection process according to the Ashby approach.

consideration or some not-examined aspect such as recyclability or availability. Fig. 1 illustrates this sequence.

The constraints are specified by the materials properties which are important to the application and also by dimension requirements of the component. The Ashby method proposes the graphical representation of materials properties in Cartesian axes, using logarithmic scales. This procedure allows one to explore two different properties simultaneously and to evaluate the performance of a given material in respect to these properties. This graphical representation is known as Ashby chart or material property chart. It is considered a powerful tool to the selection of engineering materials, granting for the analysis of different inter-related properties in a simple and rapid way. Then, the constraints are translated into attribute limits which are plotted as horizontal or vertical lines on the material selection chart. By evaluating the materials which do not meet the technical requirements established by the constraints the screening step is thereby easily conducted.

The ranking of the remaining candidates is based on the objective(s), always seeking to maximize a given performance. Ashby proposes that the objectives define material indices, for which extreme values are sought. The definition of the material indices is done by the derivation of an objective function. This function has the form shown in Eq. (1):

$$P = f(F, G, M) \tag{1}$$

P stands for the performance of the material which is a function (f) of three different elements: functional requirements (F) that are often some measurable quantity not directly expressing a material property. Examples are the heat flux through a bar, the load it carries, the temperature at which it is exposed, the electrical current flowing through it and so on. The second element encompasses the geometric parameters (G) of the component such as length, diameter, thickness or width. The last element comprises the materials properties (M), forming the so-called material index. Deriving M involves the identification of proper equations relating the materials properties that are relevant to the application under study. Ashby gives a deep understanding of this procedure in [42]. Moreover, it is important to realize that the three elements in Eq. (1) are indeed separable and the equation can be written as follows:

$$P = f_1(F) \cdot f_2(G) \cdot f_3(M) \tag{2}$$

In Eq. (2) f_1, f_2 and f_3 are separate functions that can be simply multiplied. By doing this, it is assumed that the materials properties are independent from the design-related F and G elements. Thus, the selection problem is greatly simplified as it is not necessary to solve for the complete scenario, only for the materials attributes. When conflicting objectives are involved, a trade-off strategy can be undertaken. This methodology will be described and applied in Sections 4.2 and 4.3.

The chart method is classified as a screening method for materials selection. It advantageously applies as an initial screening of materials for a given engineering application. Moreover, it can be easily coupled to the field of mechanical design, being considered a simple and quick method of evaluating the performance of specific candidates. However, it is frequently regarded as a useful tool for selecting materials when only two or three criteria govern the selection process. If, though, multiple criteria are necessary to exploit the case under study, then the method is of limited applicability. Multi-criteria decision making methods can be effectively used in these cases. An excellent introduction to such methods can be found in [42]. Although the Ashby approach has limitations at dealing with multiple objectives situations [42], it successfully applies to a variety of components [53–56]. In the next sections we develop this selection strategy to screen and rank candidates for the manufacturing of bipolar plates for PEM fuel cells.

3. The strategy for selecting bipolar plates

Following the procedure depicted in the previous section, the first step of the materials selection method is translation. Then, the very first concern is to clearly identify the functions that the material will perform for the intended application. As already mentioned, bipolar plates play vital functions in a PEM fuel cell stack: to provide electrical connection between individual cells, to distribute the reactants uniformly, to mechanically support the stack and to manage heat and water flow within the stack. Bipolar plates must meet strict technical targets to properly perform these functions. This leads to the next action in the translation step, that is, to define the constraints for the application. The targets defined by the United States Department of Energy (DOE) are widely accepted as technical criteria for bipolar plates. Some of these targets are reproduced in Table 1.

Now it is noteworthy to discuss the relevance of these targets to the materials selection procedure developed in this work. Gas

Table 1
DOE technical targets for bipolar plates.

Property	Value
Flexural strength[a]	≥25 MPa
Contact resistance (at 140 N cm^{-2})	<20 mΩ cm^2
In-plane electrical conductivity	>100 S cm^{-1}
Thermal conductivity	>10 W (m K)$^{-1}$
Gas permeability	<2 × 10^{-6} cm^3 cm^{-2} s^{-1} at 80 °C and 3 atm
Corrosion resistance	<1 μA cm^{-2}

[a] Using ASTM C651 – 11 Standard Test Method for flexural strength of manufactured carbon and graphite articles using four-point loading at room temperature.

permeability is a critical issue for polymer–graphite composites but not for metallic materials. However, it is a characteristic of the molded plate and it is not related to an intrinsic attribute of the materials employed to manufacture the plate. In this respect, it depends on the processing pressure, temperature and time. Furthermore, the size, shape and relative fraction of polymer and conductive fillers in the composition is also important. Nevertheless, the chemical nature of the matrix and fillers has little, if any, influence on the final permeability. Thus, this characteristic will not be included in the subsequent analysis. In the same way, due to the intrinsic high thermal conductivity of metals, this property is more relevant for polymer–graphite composites than for metallic plates. Even so, it has been hardly evaluated in the literature. This apparent negligence probably comes from the direct proportionality between thermal and electrical conductivities of the most part of the engineering materials [42]. In this sense, if a material is a good electrical conductor, it will also conduct heat effectively. The most important yield of a PEM fuel cell is the power it generates. Therefore, it is not surprising that electrical properties are thoroughly characterized while the thermal behavior is frequently disregarded. As a consequence, due to the lack of information in the literature, thermal conductivity will not be considered in the selection process. We let implicit that the best materials regarding electrical conductivity will also meet the constraint for thermal conductivity. From the foregoing considerations, four different constraints remained: flexural strength, contact resistance, electrical conductivity and corrosion resistance.

Next, to define the objective(s) of the selection process, the following question has to be made: what should be maximized or minimized? At this point, it is essential to ponder the relative importance of the four remaining constraints to each class of materials. As already mentioned, flexural strength is not a concern for metallic materials, since its intrinsic high toughness guarantees an excellent mechanical stability for application as bipolar plates. Polymer–graphite composites are not as tough as metallic materials and flexural strength has to be carefully evaluated. The bulk electrical conductivity of metallic materials is typically between 1000 S cm^{-1} and 10,000 S cm^{-1} [42] which is perfectly suited for bipolar plates. However, the most corrosion resistant metals develop an adherent and compact oxide layer in the PEM fuel cell environment. This so-called passive layer increases the interfacial contact resistance (ICR) of the metallic surface, thus reducing the overall electrical performance of the fuel cell. In this regard, ICR is a vital property for metal-based bipolar plates. For polymer–graphite composites, though, the scenario is different. The bulk electrical conductivity of polymer–graphite composites is much lower than that of metallic materials and the composition should be conscientiously designed to attend the DOE technical target. On the other hand, ICR is not critical, since composites do not develop a highly resistive oxide layer in contact with the PEM fuel cell environment as metals do. Regarding corrosion behavior, polymer–graphite composites are often considered chemically stable in the PEM fuel cell environment. Consequently, despite indications of the possible degradation of carbon-based bipolar plates during the operation of PEM fuel cells [43,44] due to corrosion processes, corrosion resistance is often disregarded in the literature and few data are available. Conversely, corrosion resistance is crucial for metallic plates and a much wider variety of data can be found.

The aspects depicted above suggest that different objectives should be defined for different classes of materials. Hence, it seems logical to separate our selection process in two distinct parts: (i) materials selection for polymer–graphite composite bipolar plates and (ii) materials selection for metallic bipolar plates. This segregation is justified by the antagonistic behavior of each class of materials regarding the same properties. Following this idea, we will conduct two parallel selection processes.

3.1. Materials selection for polymer–graphite composite bipolar plates

Based on the preceding discussion the objectives for selecting polymer–graphite composites are: (i.a) to maximize the flexural strength and (i.b) to maximize the electrical conductivity of the bipolar plate.

3.2. Materials selection for metallic bipolar plates

By considering the typical limitations of metal-based bipolar plates the objectives have been defined as: (ii.a) to minimize the corrosion current density and (ii.b) to minimize the interfacial contact resistance.

Finally, the translation step is completed after recognizing the variables which the designer is free to choose. We promptly identify the choice of material as a free variable in the selection process. We will also let the size and shape of the bipolar plate as free variables. This assumption applies for both polymer–graphite composite and metal-based components. Thus, our focus will be on the selection of the best material for the application.

4. Results and discussion

4.1. First screening

The selection process undertaken in this work will only consider the traditional materials for bipolar plates, i.e., polymer–graphite composites and metals. Ceramics and pure polymers have intrinsic limitations which hamper their use as bipolar plates. As a consequence, these materials cannot meet the constraints on electrical and/or thermal conductivities as shown in the Ashby chart presented in Fig. 2. The chart was plotted using the CES software. The constraints are marked as solid lines in the chart. Technical ceramics are represented as yellow, vitreous ceramics as magenta, non-technical ceramics as dark yellow, elastomers as cyan, thermosetting resins as dark-blue (navy), thermoplastics as blue, polymer foams as green, wood and natural materials as olive, ferrous metals as dark cyan, and non-ferrous metals as red bubbles. Some representative materials of each of these classes are indicated in the chart. The chart shows a range of values for each property of each material. This construction results from the variable results which can be obtained for the same type of material depending on factors such as porosity for ceramics, degree of crystallinity for polymers, purity and plastic deformation for metals.

As clearly seen, all the ceramics and polymers fail at achieving the required limits for one or both properties. Some technical ceramics pass the thermal conductivity criterion but fails at achieving the electrical conductivity constraint. Tungsten carbides are the exception. Hence, this first screening step has removed ceramics and pure polymers from the subsequent analysis.

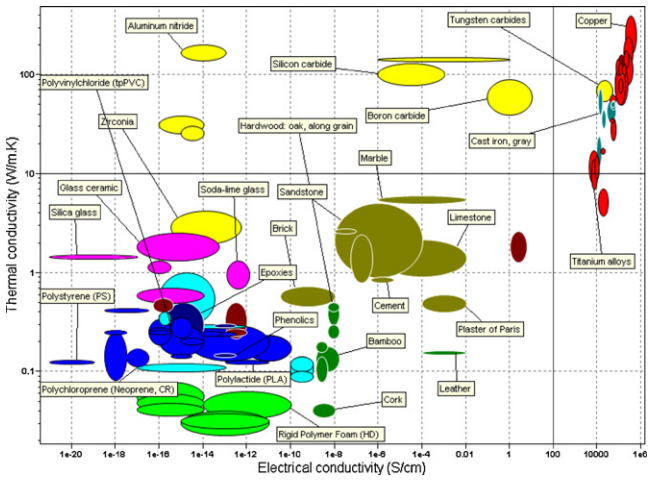

Fig. 2. Thermal conductivity-electrical conductivity chart plotted using the CES software.

Our approach for screening and ranking polymer–graphite composites and metallic materials for bipolar plates is based on the data published in the literature. The design of bipolar plates depends on specific formulations in the case of polymer–graphite composites and on proper surface treatments in the case of metals. We performed a thorough evaluation of the current literature to collect the relevant data to our materials selection process. Whenever possible, we also report on the data available for commercial bipolar plates.

4.2. Screening and ranking for polymer–graphite composites

The flexural strength-electrical conductivity chart is shown in Fig. 3. The data on the chart were collected from scientific reports and commercial products. It is important to mention that the values of electrical conductivity are referred to in-plane measurements. The number above each point denotes the reference from which the data were collected. Details about the composition of each material shown in the chart are given in Table 2. This information was not included in the chart for clarity reasons. A solid horizontal line marking the constraint on flexural strength and a solid vertical line marking the constraint on in-plane electrical conductivity are inserted in the chart. Moreover, authors often evaluate several different materials which may differ on composition, processing conditions or both. We report only the best condition achieved by the authors, assuming that this would be the proper choice for the

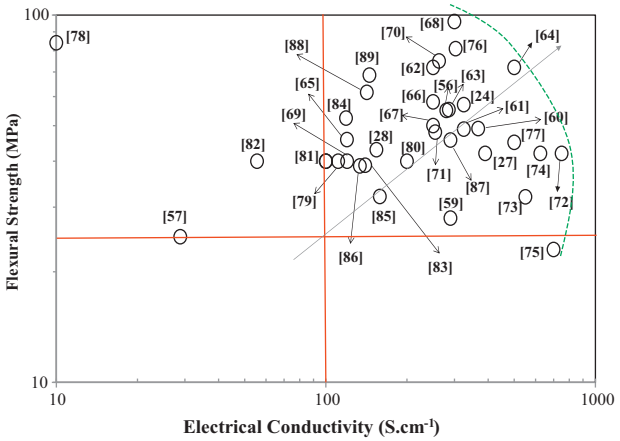

Fig. 3. Flexural strength-electrical conductivity chart.

Table 2
Composition of the bipolar plates displayed in Fig. 3.

Reference	Composition
[24]	Laminate with 25 wt.% polyphenylene sulfide (PPS) + 70 wt.% graphite + 6.0 wt.% carbon fiber
[27]	60 wt.% Graphite (60% with particle size > 90 μm and 40% with particle size < 45 μm) + 40 wt.% aluminate cement (Al_2O_3 + CaO)
[28]	25 wt.% epoxy resin + 75 wt.% compressed expanded graphite sheets (CEG)
[43]	30 wt.% phenol formaldehyde + 60 wt.% graphite + 5 wt.% carbon black + 5 wt.% carbon fiber
[57]	20 wt.% polyvinylidene fluoride (PVDF) + 80 wt.% Ti_3SiC_2
[58]	Commercial vinyl ester based composite bipolar plate (no further details available in the datasheet)
[59]	60 wt.% graphite + 40 wt.% aluminate cement (Al_2O_3 + CaO)
[60]	60 wt.% graphite + 40 wt.% aluminate cement (Al_2O_3 + CaO) – graphite particle size < 45 μm
[61]	Laminate with 25 wt.% PPS + 70 wt.% graphite + 6.0 wt.% carbon fiber
[62]	35 vol.% phenolic resin (novolac) + 25 vol.% carbon black + graphite + carbon fiber
[63]	40 wt.% phenolic resin (novolac) + 60 wt.% expanded graphite (50% with particle size 50 μm + 50% with particle size 300 μm)
[64]	50 wt.% epoxy resin + 50 wt.% expanded graphite
[65]	30 wt.% epoxy resin + 70 wt.% expanded graphite
[66]	15 wt.% phenolic resin (novolac) + 85 wt.% graphite (flake; particle size 25 μm)
[67]	25 wt.% phenolic resin (novolac) + 7.5 wt.% expanded graphite + 67.5 wt.% graphite (flake)
[68]	23 wt.% polyphenylene sulfide (PPS) + 70 wt.% graphite + 7.0 wt.% carbon fiber
[69]	15–20 wt.% epoxy resin + 80–85 wt.% graphite
[70]	Phenolic resin (novolac) + graphite + carbon black + carbon fiber
[71]	25 vol.% epoxy resin + 61 vol.% graphite + 5.0 vol.% carbon black + 2 vol.% multi-walled carbon nanotubes + 7.0 vol.% carbon fiber
[72]	30 wt.% vinyl ester resin + 70 wt.%graphite + 2 phr multi-walled carbon nanotubes
[73]	20 wt.% polypropylene + 80 wt.% graphite + 4 phr multi-walled carbon nanotubes
[74]	30 wt.% vinyl ester resin + 2.0 wt.% multi-walled carbon nanotubes + 68 wt.% graphite
[75]	Sintered mesocarbon microbead (MCMB) plate from a suspension with a solid loading of 66.7 wt.%
[76]	25 vol.% phenolic resin + 65 vol.% graphite + 2.5 vol.% carbon fiber + 7.5 vol.% carbon black
[77]	35 vol.% phenolic resin (resole) + 50 vol.% graphite + 5.0 vol.% carbon fiber + 10 vol.% carbon black
[78]	43.7 wt.% polyphenylene sulfide (PPS) + 43.8 wt.% graphite + 4.0 wt.% carbon fiber + 8.5 wt.% carbon black
[79]	Commercial plate – composition non specified in the datasheet
[80]	Commercial phenolic resin based composite bipolar plate (no further details available in the datasheet)
[81]	Commercial polyvinylidene fluoride (PVDF) based composite bipolar plate (no further details available in the datasheet)
[82]	Commercial polypropylene based composite bipolar plate (no further details available in the datasheet)
[83]	70 wt.% expanded graphite + 30 wt.% aromatic polydisulfide
[84]	20 wt.% polyphenylene sulfide (PPS) + 80 wt.% graphite
[85]	50 wt.% poly(arylene disulfide) + 50 wt.% graphite nanosheet
[86]	20 wt.% polyphenylene sulfide (PPS) + 80 wt.% mesocarbon microbeads
[87]	25 wt.% vinyl ester resin + 75 wt.% graphite + 2 phr montmorillonite (MMT)
[88]	15 wt.% phenolic resin + 85 wt.% graphite
[89]	3 wt.% carbon nanotube (Fentom/UV treated) + 14.54 wt.% phenolic resin + 82.46 wt.% graphite

manufacturing of the bipolar plate, according to the published data. It is worth mentioning that this chart is based on the same principles of the CES software but was not plotted using it. The materials displayed in the chart are specific formulations developed by several top research groups throughout the world. The CES software version used to plot the chart in Fig. 2 does not contain such information. Then, we chose to use the representation shown in Fig. 3. It is perfectly suited to the materials selection process developed in

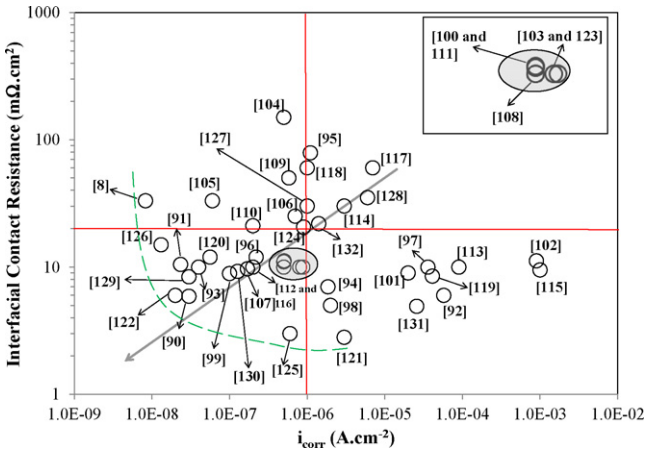

Fig. 4. Interfacial contact resistance-corrosion current density chart.

this text. The chart shown in next section (Fig. 4) follows the same philosophy.

Based on both constraints the search region is given by the first quadrant of the chart shown in Fig. 3. This region comprises the vast majority of the data. Only the candidates [57,75,78,82] are screened. Let us analyze each material separately. As seen in Table 2, the bipolar plate material described in [57] was comprised of a mixture of PVDF and titanium silicon carbide (Ti_3SiC_2). As seen in Fig. 3 it stands in the limit of the constraint on flexural strength and is significantly lower than the constraint on electrical conductivity. At a first sight this result could indicate that the composite would not be suitable for application as bipolar plate. However, this conclusion oversimplifies the problem. It is known [26] that the flexural strength and electrical conductivity of carbon based composites for bipolar plates depend on a variety of factors such as the conductive filler particle size and dispersion within the polymer matrix, volume fraction of each component and processing conditions. Therefore, as highlighted by the authors, it is possible to increase the performance of the PVDF–Ti_3SiC_2 composite by a proper optimization of the Ti_3SiC_2 content, Ti_3SiC_2 particle size and the molding conditions. This approach has been practiced by the same group in a more recent publication [27]. The performance of the PVDF–Ti_3SiC_2 composite was significantly improved regarding both flexural strength and electrical conductivity by selecting a suitable combination of filler content and particle size. The plate described in [75] was prepared from a suspension of mesocarbon microbeads (MCMB) with a solid loading of 66.7 wt.%, sintered at 1100 °C in an inert atmosphere. It is observed that the electrical conductivity was excellent, only surpassed by the result shown in [72]. However, the flexural strength was slightly lower than the constraint of 25 MPa. Notwithstanding this lack of mechanical stability, careful control of the solid loading in the original suspension and/or the sintering conditions could enhance the mechanical properties of the finished part, thus surpassing the constraint on flexural strength. Alternatively, MCMB particles could be used as conductive fillers for the preparation of composite plate by dispersing them within a proper organic matrix. In fact, this approach was successfully employed by Yang and Shi [86]. They developed polyphenylene sulfide (PPS)–MCMB composite bipolar plates with superior flexural strength. In comparison with [75] the electrical conductivity was sacrificed due to the incorporation of the insulating polymer matrix. In spite of the increased insulating character, the composite still surpassed the constraint on electrical conductivity as shown in Fig. 3. The plate developed in [78] presents outstanding flexural strength but the electrical conductivity is far below the constraint of 100 S cm^{-1}. As shown in Table 2, this composite comprises a mixture of PPS, graphite, carbon fiber and carbon black. The superior mechanical behavior probably arises from the high content of the polymer matrix and from the carbon fibers. In the same way, the low electrical conductivity is a consequence of the high PPS content (43.7 wt.%). The performance of the composite can be drastically altered through an appropriate balance between the volume fractions of each component in the mixture. PPS has proved to meet the constraints on both flexural strength and electrical conductivity, depending on its relative content in the composite bipolar plate as seen in [24,61,68,84,86]. Finally, the commercial polypropylene-based composite bipolar plate identified as [82] in Fig. 3 displays suitable flexural strength but low electrical conductivity. This could indicate that polypropylene should not apply as the matrix for composite bipolar plates. Indeed, it does not appear as the most frequent polymer matrix within the best composite bipolar plates. A careful analysis of Table 2 confirms this assumption. Yet, the electrical conductivity of polypropylene-based composite bipolar plates can be tailored to meet the constraint of 100 S cm^{-1}. Liao et al. [73] achieved this goal by introducing multi-walled carbon nanotubes (MWNTs) into a polypropylene–graphite mixture.

The selection process screened only four candidates. The search region (first quadrant) encompasses 33 candidates. Next step is to define how to rank these materials regarding the objectives previously defined: to maximize the flexural strength and the electrical conductivity. These are conflicting objectives for a composite bipolar plate. An increment of flexural strength is often related to the increase of the insulating polymer matrix content. As a result, the electrical conductivity diminishes. This conflict can be easily managed through the trade-off strategy proposed by Ashby [42]. Following this methodology, the choice of material that maximizes both properties simultaneously is based on the definition of a solution that meets all the constraints but is not necessarily optimal by either of the objectives. Each bubble in the first quadrant of Fig. 3 is a solution to the selection process. The solutions that maximize flexural strength do not maximize electrical conductivity and vice versa. The arrow points in the direction of the solution, giving the best compromise between the two objectives. This solution is given by Ref. [64]. From this solution a line or surface can be traced in which other solutions also lie. This surface is called the optimal trade-off surface. It is not mathematically defined. The trade-off surface is arbitrarily traced from the following procedure: after identifying the solution that gives the best compromise between the two objectives (Ref. [64] in our case), a tangent line is traced from this point, extending to the highest (or smallest, depending on the objective) values of each material property shown in the chart. This line must be tangential to the most external solutions. Other solutions can lie exactly on this trade-off surface. As shown in Fig. 3 the solutions that lie on the trade-off surface are [64,68,72]. These solutions are called non-dominated solutions. Solutions that lie more internally are dominated by others. Ranking the materials that lie on the trade-off surface requires a further step. The definition of what is the best material for the application is mathematically determined by a linear penalty function (Z) as expressed in Eq. (3):

$$Z = \alpha_1 \cdot P_1 + \alpha_2 \cdot P_2 \tag{3}$$

The best material gives the smallest value of the penalty function. In Eq. (3) P_1 and P_2 are called performance metrics. These parameters are related to the objectives of the selection process. As we seek for the lowest value of Z, in our case the values of P_1 would be the inverse of the flexural strength, whereas the values of P_2 would be the inverse of the electrical conductivity. The parameters α_1 and α_2 are called exchange constants. The values of these constants depend on the relative importance given to each objective. If both objectives have the same relative importance, then α_1 is equal to α_2. If the designer gives more importance to one objective

relative to the other, then the constants assume different values. The definition of the values of the exchange constants is arbitrary, depending on specific needs for the application, as defined by the designer. In our selection process we give the same relative importance to each objective. The same procedure will be adopted for the selection of metallic bipolar plates. The arrow shown in Fig. 3 is an indication of the direction that minimizes the values of Z. It is not mathematically defined, being only a visual trace to point the optimal solutions to the selection process.

As already mentioned, [64,68,72] are the best candidates for the application. The more external solution, [64], is the non-dominated solution of the process (the best candidate). Refs. [68,72] are dominated by [64]. If one calculates the Z values for [68,72] (given that $\alpha_1 = \alpha_2$), then [68] is the second and [72] is the third choice. A second group of materials lies more internally [73,74,76,77], representing the next best choices after those that lie exactly on the trade-off surface. These materials are selected by inspecting the chart and determining the distance of each material to the trade-off surface. The same procedure of identifying the dominating solutions and calculating Z values can be applied to rank these candidates and the next.

At this point, it is imperative to expand the discussion by carefully evaluating the composition of these plates. The composite investigated in [64] was comprised of a mixture of equal fractions of epoxy resin and expanded graphite. In Ref. [68] the plate was prepared from a proper mixture of PPS, graphite, carbon fiber and carbon black. Vinyl ester resin, graphite and multi-walled carbon nanotubes comprised the mixture developed in [72]. A common feature to these composites is the use of an organic matrix with a polar group in the backbone. Polymers with polar atoms or a single electron or pair of single electrons in their molecular configuration are easy to polarize or delocalize. As a consequence, the formation of electrical channels is favored, thus enhancing the electrical conductivity of the composite [73]. This behavior is confirmed through the analysis of the composition of the second set of candidates. The polymer matrix employed as the binder to the conductive fillers in composite developed in [74] was a vinyl ester resin. Graphite and MWNTs complete the formulation. For both [76,77] the composites were prepared from a mixture of phenolic resin, graphite, carbon black and carbon fiber. Phenolic resin is a typical example of polymer in which the electrical conductivity is governed by the polar groups in the molecule [26]. The only exception is the composite described in [73], where the binder is a non-polar molecule (polypropylene). In this case graphite and MWNTs were used as conductive fillers.

From this point, further considerations should be made. The use of polar group-containing polymer matrices is beneficial but is not the only factor to be considered in the selection process. In Ref. [65], for instance, the composite was prepared with epoxy resin and expanded graphite, similarly to Ref. [64]. However, the manufacturing method was different. While an intercalation method was used to prepare the composite in [64], a compression–impregnation–compression method was developed in [65]. The difference between the electrical and mechanical performance of each composite is significant as seen in Fig. 3. It is noteworthy that the addition of MWNTs is beneficial to the electrical conductivity of the composites. The three highest conductive plates in the search region (first quadrant) are [72–74]. MWNTs are present in all these composites. Nevertheless, the dispersion of MWNTs within the polymer matrix is dependent on both the content and surface treatment of the nanometric filler. Different treatments may lead to completely distinct results for the same type of MWNT. In Refs. [71,89], for instance, MWNTs were also added to the composite but the electrical performance was not as good as those reached by the composites shown in [72–74]. Carbon fiber is important to maximize the flexural strength of the composites. The highest mechanical stability was found for the composites developed in [68,76]. Carbon fibers are present in both materials.

The complexity of the materials selection process of carbon based composite bipolar plates was depicted above. Our results yielded the materials developed in [64,68,72] as the best candidates for this application. As seen, three different polymer matrices were used: epoxy resin as the binder in [64], PPS in [68] and a vinyl ester resin in [72]. The highest conductivity was found for the composite in [72] whose composition contains MWNTs. The highest flexural strength was found for the composite in [68] whose composition contains carbon fibers. The composite in [64] gives a balance between flexural strength and electrical conductivity. From these observations some useful guidelines can be identified: (i) the selection of a polymer matrix containing polar groups in the backbone is beneficial to the electrical conductivity; (ii) the incorporation of properly dispersed MWNTs enhances the electrical conductivity; and (iii) carbon fibers can be effectively employed to improve the flexural strength. The bipolar plate designer should be aware of these guidelines and, most importantly, should be capable of combining this information with the careful control of processing conditions and relative fractions of each component in the composite formulation.

4.3. Screening and ranking for metallic bipolar plates

The ICR-corrosion resistance chart is shown in Fig. 4. The data on the chart were collected from scientific reports. The corrosion resistance is represented by the corrosion current density (i_{corr}) determined from potentiodynamic polarization curves. The experiments are conducted in a variety of different electrolytes, aiming at simulating the best as possible the actual conditions of a PEM fuel cell environment. In this regard, it is a common practice to perform the corrosion tests in a H_2SO_4 aqueous solution with the addition of traces of HF at 70 °C or 80 °C. We do not mention the different electrolytes used in each reference, assuming that small variations in both composition and temperature would not be relevant to the selection process. The ICR values are referred to a 20 kg cm^{-2} contact pressure. The number above each point denotes the reference from which the data were collected. Details about the core material and coating/surface treatment of each corresponding bipolar plate material shown in the chart are given in Table 3. This information was not included in the chart for clarity reasons. A solid horizontal line marking the constraint on ICR and a solid vertical line marking the constraint on corrosion resistance are inserted in the chart. The inset is an expansion of the region circled near the intersection between the two lines that mark the constraints. Five different materials lie in this region. The inset allows for a clearer identification of their relative positions in the chart. In this chart, the objectives are to minimize both ICR and i_{corr}. Therefore, the third quadrant is the search region.

The screening step eliminates various candidates as observed in Fig. 4. The candidates screened based on the constraint on ICR [8,95,104–106,109,117,125] are in the second quadrant of the chart. Those screened due to the constraint on corrosion resistance are in the fourth quadrant of the chart [92,94,97,98,101,102,34,114,118,120,129,130]. The materials in [113,116,126] are screened due to both constraints.

Initially, let us analyze the materials screened due to the constraint on ICR. The core materials were austenitic stainless steels (304, 310S, 316L and 317L). Only in Ref. [104] the surface metallic plate was not protected from the PEM fuel cell environment, exposing the bare substrate (310S stainless steel) to it. The other seven materials underwent some surface treatment. Cha et al. [8] deposited a NbN/NbCrN coating in a 304 stainless steel substrate and observed an excellent corrosion resistance. As seen in Fig. 4

Table 3
Core material and surface treatments of the metallic bipolar plates displayed in Fig. 4.

Reference	Core material	Surface treatment
[8]	304 stainless steel	NbN/NbCrN coating (inductively coupled plasma assisted d.c. magnetron sputtering)
[90]	1045 carbon steel	Rolling followed by pack chromization at 700 °C for 2 h
[91]	1020 carbon steel	Ni electroplating + pack chromization at 700 °C for 2 h
[92]	Al-5083 alloy	5 μm CrN coating deposited by cathodic arc evaporation physical vapor deposition
[93]	Hastelloy® G-35™	Nitridation at 1100 °C for 6 h
[94]	316L stainless steel	Carbon film deposited by close field unbalanced magnetron sputtering ion plating
[95]	316L stainless steel	Silver ion implantation
[96]	Ti (purity of 99.6%)	Nitrogen plasma immersion ion implantation
[97]	$Fe_{41}Cr_{18}Mo_{14}Y_2C_{15}B_6N_4$	–
[98]	316L stainless steel	CrN coating produced by pulsed bias arc ion plating ($Cr_{0.49}N_{0.51}$)
[99]	304 stainless steel	Carbon coating (plasma assisted chemical vapor deposition)
[100]	304 stainless steel	CrN/Ti multilayer coating (cathodic arc plasma deposition)
[101]	$Fe_{43}Cr_{18}Mo_{14}C_{15}B_6Y_2Al1N1$	–
[102]	18Cr–12Ni–2Mo–3W stainless steel	–
[103]	446M stainless steel	Immersion in 15 wt.% HCl solution for 5 min + heat treatment in ambient air at 380 °C for 10 min
[104]	310S stainless steel	–
[105]	316L stainless steel	Electrochemical treatment in a CeO_8S_2 solution for Ce insertion into the passive film
[106]	316L stainless steel	Polyamide-imide (PAI)-carbon black composite coating (40 wt.% PAI + 60 wt.% carbon black)
[107]	304 stainless steel	Carbon nanotube coating + polypropylene–carbon black-carbon fiber composite (40 wt.% polypropylene + 50 wt.% carbon black + 10 wt.% carbon fiber)
[108]	310S stainless steel	TiN nanoparticle coating (electrophoretic deposition)
[109]	316L stainless steel	Nitridation (Cr_2N layer) at 1100 °C for 2 h of a previously electroplated Cr layer
[110]	316L stainless steel	CrN coating (physical vapor deposition)
[111]	304 stainless steel	Nitride layer (physical vapor deposition)
[112]	316L stainless steel	Plasma nitriding at 370 °C for 2 h
[34]	304L stainless steel	Glow discharge plasma nitriding at 370 °C for 2 h
[113]	316L stainless steel	Cr interlayer + CrN top-coat (physical vapor deposition)
[114]	349 stainless steel	Nitridation at 1100 °C for 7 h
[115]	446 stainless steel	Nitridation 1100 °C for 2 h
[116]	446 stainless steel	–
[117]	317L stainless steel	SnO_2:F coating (low pressure chemical vapor deposition)
[118]	430 stainless steel	Nb cladding
[119]	420 stainless steel	Pack chromization at 700 °C for 2 h
[120]	316L stainless steel	$Cr_{0.23}C_{0.77}$ coating (pulsed bias arc ion plating)
[121]	Fe–27Cr–6V	Nitridation at 850 °C for 24 h
[122]	316L stainless steel	–
[123]	316L stainless steel	–
[124]	316 stainless steel	ZrN film (physical vapor deposition) + 10 nm Au top coat (electroplating)
[36]	304 stainless steel	TiN (pulsed bias arc ion plating)
[125]	316L stainless steel	TiN (multi-arc ion plating)
[126]	316L stainless steel	Cr/CrN/Cr multilayer (pulsed bias arc ion plating)
[127]	316L stainless steel	CrN/Cr coating (pulsed bias arc ion plating)
[128]	304 stainless steel	NbN film (plasma surface diffusion alloying method)
[129]	304 stainless steel	Carbon film (close field unbalanced magnetron sputtering ion plating)
[130]	316L stainless steel	CrN film (electron beam physical vapor deposition)

the i_{corr} of this material is the lowest in chart. However, the ICR was above the constraint. According to the authors, this property may be improved by controlling the gas ratio ($N_2/(Ar + N_2)$) used in the deposition process. Feng et al. [95] employed Ag-ion implantation to modify the surface a 316L stainless steel plate. Although both ICR and corrosion resistance have been improved compared with the bare substrate, ICR was still higher than the constraint of 20 mΩ cm^2. The authors did not suggest how to modify the implantation process in order to achieve better ICR performance. The same group performed ion implantation with carbon ions [131] and nickel ions [132] with stainless steel bipolar plates. Despite the significant decrease of ICR in comparison with the untreated metallic surface, the values (not shown in Fig. 4) did not meet the constraint of 20 mΩ cm^2. In another reference, though, these authors achieved 22.1 mΩ cm^2 for the ICR of a 316L stainless steel bipolar plate co-implanted with Ni—Cr and cobalt [31]. The value is very close to the active constraint on this property. It seems, therefore, that ion implantation is not at a mature level, but is very promising for improving the surface properties of metallic bipolar plates by properly selecting ion nature and fluence. Lavigne et al. [105] have found that a Ce-based electrochemical treatment of 316L stainless steel surface enhanced its corrosion resistance and decreased the ICR. Nevertheless, the value was higher than the ICR constraint and the authors did not indicate how to achieve further improvements for this property. Lee and Lim [106] developed a composite PAI–carbon black coating to improve the performance of a 316L stainless steel bipolar plate. As seen in Fig. 4, neither ICR nor corrosion resistance are outstanding. They suggest that the relative fraction of carbon black in the film should be carefully controlled in order to achieve low ICR and high corrosion resistance simultaneously. The negative influence of the insulating PAI component in the composite contributes to the high ICR value. Thus, it can be inferred that this approach is not suitable to produce low ICR bipolar plates. Any insulating component should be avoided. The nitridation process employed by Nam and Lee [109] did not provide suitable ICR performance for a 316L stainless steel bipolar plate. The corrosion resistance of nitride layers can also not meet the constraint in the chart. This is the case of Refs. [34,114]. However, nitridation has been effectively employed by other authors [111,112]. The structure of the nitrided layer depends on the processing conditions such as the treatment temperature and time. In this regard, different behaviors may be expected depending on specific parameters. The SnO_2:F coating on the 317L stainless plate in [117] and the TiN coating on 316L stainless steel plate in [125] presented the same problem regarding the constraint on ICR. While SnO_2:F coatings have not been successfully developed by any other group regarding their ICR performance, TiN coatings have shown to meet both the ICR and corrosion

resistance constraints [108,36], depending on the deposition method.

The materials in [113,126] have the same core metal (316L stainless steel) with different Cr and CrN multi-layered coatings prepared by physical vapor deposition (PVD) methods. As seen, these materials, despite improving the performance of the bare substrate, did not meet both constraints. However, one should not disregard this approach as a viable alternative of attaining surface-effective metallic bipolar plates. Zhang et al. [127], for instance, used a PVD (pulsed bias arc ion plating) to deposit a CrN/Cr multilayer film on the surface of a 316L stainless steel plate. The resulting material met both the ICR and corrosion resistance constraints being amongst the best candidates in the chart as shown in Fig. 4. Therefore, the relative unsuitable performance of [113,126] should be rather envisaged as an opportunity of improving both ICR and corrosion resistance through the conscientious investigation of specific processing parameters. Corrosion resistance problems arising from PVD methods have been displayed by the bipolar plates developed in [92,94,101,34,120,129,130]. A common feature to these references is that the PVD coatings were comprised of monolayers. The control of coating defects is of prime importance to avoid the onset of corrosion due to the penetration of the electrolyte through these pathways. Multi-layered PVD films are less prone to this phenomenon [133].

Unmodified metallic surfaces generally lack both corrosion resistance and surface conductivity, presenting high ICR and i_{corr} values. This behavior is shown in several of the references marked in the chart shown in Fig. 4. We do not display all these values in the chart, as they do not bring new knowledge to the selection process. We preferred to show only less usual materials such as the metallic glasses in [97,101]. These materials, despite the low ICR, are not suitable to bipolar plate applications due to the high i_{corr} values. The same finding is observed for the tungsten-modified austenitic stainless steel in [102]. The presence of tungsten in the passive film decreased the ICR value, but the corrosion resistance is far too low for a bipolar plate. The 446 ferritic stainless steel in [116] presented excessive ICR and i_{corr} values. Exceptions to the overall poor performance of untreated metallic bipolar plates can be found in the studies conducted by Yang et al. [122,123]. They tested 316L stainless steel specimens in the cathode environment of a PEM fuel cell under different conditions of temperature and acidity. As observed in Fig. 4, the results from these references are near the limits of both constraints. Nevertheless, this is not an indication that bare 316L stainless steel is able to perform well in a PEM fuel cell environment. In fact, there is no registration of proper performance of untreated metallic alloys in the literature. The surface condition is more important to the performance of the metallic bipolar plate than the core material. In this regard, the final behavior will be a function of the composition and structure of the coating layer or passive film on the surface of the core material.

From the 44 candidates shown in Fig. 4, only 21 remained to be ranked. As described for the chart flexural strength-electrical conductivity (Section 4.2), the ranking step for the chart ICR-corrosion resistance will also be conducted through the approach based on conflicting objectives by means of the definition of a trade-off surface. ICR and corrosion resistance are conflicting properties, since an increase of corrosion resistance (decreasing i_{corr}) is often associated with a less conductive surface (with high ICR). This is a serious drawback of metallic materials regarding their use as bipolar plates, as the corrosion resistance typically comes from the development of a low conductivity oxide layer (passive film) with intrinsically high ICR. In this context, the choice of material that minimizes both properties simultaneously is based on the definition of a solution that meets all the constraints but is not necessarily optimal by either of the objectives. Each bubble in the third quadrant of Fig. 4 is a solution to the selection process. The solutions that minimize ICR do not minimize i_{corr} and vice versa. The arrow points to the solution that gives the best compromise between the two objectives. This solution is given by Ref. [121]. From this point a line or surface can be traced in which other solutions also lie. This surface is the optimal trade-off surface for the chart ICR-corrosion resistance. The solutions that lie on this surface are [121,124,36]. As already mentioned, if the same relative importance is given to each objective, [121] represents the best candidate to the application. A second group of materials lies more internally [90,91,93,119,127], representing the next best choices after those that lie on the trade-off surface. The top ranked bipolar plate was a vanadium modified Fe—27Cr alloy nitrided at 850 °C for 24 h. The nitridation process yielded the formation of a conductive surface layer of V-doped CrN which accounts for the high corrosion resistance and low ICR of the nitrided material. This approach is unique in the literature. Nitridation has also yielded good results for a Ni—Cr alloy (Hastelloy® G35™) [93]. The low contact resistance of the plate in [124] is due to a gold layer applied onto a PVD ZrN coated-316 stainless steel. As observed in Fig. 4, this material presents the lowest ICR at the trade-off surface, but its corrosion resistance is relatively poor in comparison with [121,36]. The presence of the conductive gold top layer proved to be effective at reducing the ICR. In [36] a PVD TiN single layer was deposited on a 304 stainless steel providing exceptionally low i_{corr}, while the ICR is not as good as the corrosion resistance. The bipolar plate developed in [90] gives the second best performance owing to a compromise between ICR and i_{corr}. This plate was manufactured with low cost 1045 carbon steel previously subjected to rolling to activate the surface and, then, to low-temperature pack chromization at 700 °C for 2 h. The same research group has achieved excellent results in [91] by using this approach with 1020 carbon steel. However, in [91] the carbon steel plate was first electroplated with Ni and then chromized. Pack chromization has also been successfully employed by Wen et al. [119] with martensitic type 420 stainless steel, giving a good balance between ICR and i_{corr}. Zhang et al. [127] produced a high performance 316L stainless steel plate coated with a PVD multi-layered CrN/Cr coating. According to Fig. 4, this material gives the third best compromise between ICR and i_{corr}.

From the above standings the three top ranked candidates may be defined as follows: [121] > [90] > [127]. This result evidences that the core metallic material used for manufacturing bipolar plates may be even an intrinsically low corrosion resistant alloy such as 1045 carbon steel [90], if a proper surface modification technique is employed. In this context, as the surface of the metallic material is responsible the final performance of the bipolar plate, the materials selection process allows the following recommendations: pack chromization gives attractive results as shown by Bai et al. [90,91] and by Wen et al. [119]. Nitridation is also an interesting route as well as PVD methods that yield multi-layered structures based especially on low resistivity nitride compounds. A common feature to the most successive treatments is the formation of a coating layer comprised of Cr-containing and/or N-containing compounds. Moreover, the structure of the protective films must be carefully designed by the selective definition of processing parameters in order to avoid the formation of through-coating defects that would hamper the anticorrosion properties of the coating.

5. Conclusions

The Ashby approach was employed for selecting materials for the manufacturing of bipolar plates for PEM fuel cells. The selection process was divided into two distinct parts: selection of materials for polymer–graphite composite bipolar plates and for metallic-based ones. These routes were defined based on the different attributes relevant to each type of material. The process is highly

complex due to the several simultaneous aspects involved in the performance of bipolar plates. Notwithstanding its simplicity, the Ashby approach proved to be effective, evidencing the weaknesses and strengths of particular options. A critical understanding of the application could be delineated and useful guidelines could be drawn. In this context, the following bullet points can be highlighted:

- The objectives for selecting materials for polymer–graphite composite plates are to maximize both electrical conductivity and flexural strength. These objectives are conflicting. As a consequence, a trade-off strategy applies.
- The top ranked materials for composite bipolar plates were those described in Refs. [64,68,72]. A common feature to these candidates was the use of a polymer matrix containing polar groups in the backbone. This characteristic was identified as highly beneficial for the electrical conductivity of the composites. Phenolic, epoxy and vinyl ester thermosetting resins and the thermoplastic PPS are remarkable options.
- Furthermore, the incorporation of properly dispersed MWNTs enhances the electrical conductivity and carbon fibers can be effectively employed to improve the flexural strength. The compromise between electrical conductivity and flexural strength depends on the meticulous use of these fillers, in addition to the polymer–graphite base material.
- The objectives for selecting materials for metallic bipolar plates are to minimize both interfacial contact resistance and corrosion current density. A trade-off strategy could be employed due to the conflicting nature of these objectives.
- The top ranked materials for metallic bipolar plates were those described in Refs. [121,90,127]. The surface treatment is more important than the core metallic alloy owing to the performance of the bipolar plate. Even an intrinsically low corrosion resistant alloy such as 1045 carbon steel can be effectively employed as a bipolar plate since it receives the proper surface treatment as shown in [90].
- Cr and/or N-containing coatings are the most attractive materials for top layers on metallic bipolar plates. Pack chromization, nitridation and PVD-based multi-layered films may yield high performance surfaces.

Acknowledgements

The authors are grateful to CNPq (The Brazilian Research Council) for the financial support to this work (Project 558134/2008-4). Mara C. L. de Oliveira is thankful for the post-doctoral grant (Proc. 150396/2009-0).

References

[1] S.S. Dihrab, K. Sopian, M.A. Alghoul, M.Y. Sulaiman, Renew. Sustain. Energy Rev. 13 (2009) 1663–1668.
[2] X. Zhang, S.H. Chan, G. Li, H.K. Ho, J. Li, Z. Feng, J. Power Sources 195 (2010) 685–702.
[3] S.J. Peighambardoust, S. Rowshanzamir, M. Amjadi, Int. J. Hydrogen Energy 35 (2010) 9349–9384.
[4] P. Corbo, F. Migliardini, O. Veneri, Int. J. Hydrogen Energy 32 (2007) 4340–4349.
[5] J.J. Hwang, W.R. Chang, F.B. Weng, A. Su, C.K. Chen, Int. J. Hydrogen Energy 33 (2008) 3801–3807.
[6] X.-Z. Yuan, H. Li, S. Zhang, J. Martin, H. Wang, J. Power Sources 196 (2011) 9107–9116.
[7] R.A. Antunes, M.C.L. Oliveira, G. Ett, V. Ett, Int. J. Hydrogen Energy 35 (2010) 3632–3647.
[8] B.-C. Cha, Y.-Z. You, S.-T. Hong, J.-H. Kim, D.-W. Kim, B.-S. Lee, S.-K. Kim, Int. J. Hydrogen Energy 36 (2011) 4565–4572.
[9] H. Zhang, M. Hou, G. Lin, Z. Han, Y. Fu, S. Sun, Z. Shao, B. Yi, Int. J. Hydrogen Energy 36 (2011) 5695–5701.
[10] C. Turan, O.N. Cora, M. Koç, Int. J. Hydrogen Energy 36 (2011) 12370–12380.
[11] Y. Wang, K.S. Chen, J. Mishler, S.C. Cho, X.C. Adroher, Appl. Energy 88 (2011) 981–1007.
[12] R. Boddu, U.K. Marupakula, B. Summers, P. Majumdar, J. Power Sources 189 (2009) 108301092.
[13] Y. Wang, S. Basu, C.-Y. Wang, J. Power Sources 179 (2008) 603–617.
[14] S. Lee, H. Jeong, B. Ahn, T. Lim, Y. Son, Int. J. Hydrogen Energy 33 (2008) 5691–5696.
[15] Y. Wang, C.-Y. Wang, J. Power Sources 147 (2005) 148–161.
[16] A. Iranzo, M. Muñoz, E. López, J. Pinto, F. Rosa, Int. J. Hydrogen Energy 35 (2010) 11437–11447.
[17] M. Matian, A. Marquis, N. Brandon, Int. J. Hydrogen Energy 36 (2011) 6051–6066.
[18] Y. Wang, C.-Y. Wang, J. Power Sources 153 (2006) 130–135.
[19] X. Li, I. Sabir, Int. J. Hydrogen Energy 30 (2005) 359–371.
[20] C.-Y. Wang, Chem. Rev. 104 (2004) 4727–4766.
[21] H. Meng, C.-Y. Wang, J. Electrochem. Soc. 151 (2004) A358–A367.
[22] Y. Wang, J. Power Sources 185 (2008) 261–271.
[23] R. Roshandel, F. Arbabi, G.K. Moghaddam, Renew. Energy 41 (2012) 86–95.
[24] B.D. Cunningham, D.G. Baird, J. Power Sources 168 (2007) 418–425.
[25] N.P. Brandon, S. Skinner, B.C.H. Steele, Appl. Rev. Mater. Res. 33 (2003) 183–213.
[26] R.A. Antunes, M.C.L. De Oliveira, G. Ett, V. Ett, J. Power Sources 196 (2011) 2945–2961.
[27] S. Chunhui, P. Mu, Y. Runzhang, Int. J. Hydrogen Energy 33 (2008) 1035–1039.
[28] C. Du, P. Ming, M. Hou, J. Fu, Y. Fu, X. Luo, Q. Shen, Z. Shao, B. Yi, J. Power Sources 195 (2010) 5312–5319.
[29] J.W. Kim, N.H. Kim, T. Kuilla, T.J. Kim, K.Y. Rhee, J.H. Lee, J. Power Sources 195 (2010) 5474–5480.
[30] S.R. Dhakate, S. Sharma, N. Chauhan, R.K. Seth, R.B. Mathur, Int. J. Hydrogen Energy 35 (2010) 4195–4200.
[31] K. Feng, Y. Shen, D. Liu, P.K. Chu, X. Cai, Int. J. Hydrogen Energy 35 (2010) 690–700.
[32] A. Hermann, T. Chaudhuri, P. Spagnol, Int. J. Hydrogen Energy 30 (2005) 1297–1302.
[33] A.M. Lopez, F. Barreras, A. Lozano, L. Gonzalez, J.A. Garcia, L. Valino, R. Mustata, J. New Mater. Electrochem. Syst. 12 (2009) 97–102.
[34] H. Wang, G. Teeter, J.A. Turner, J. Fuel Cell Sci. Technol. 7 (2010) 021018–021025.
[35] M.A.L. García, M.A. Smit, J. Power Sources 158 (2006) 397–402.
[36] E.A. Cho, U.-S. Jeon, S.-A. Hong, I.-H. Oh, S.-G. Kang, J. Power Sources 142 (2005) 177–183.
[37] Y. Show, M. Miki, T. Nakamura, Diamond Relat. Mater. 16 (2007) 1159–1161.
[38] S.A.A. El-Enin, O.E. Abdel-Salam, H. El-Abd, A.M. Amin, J. Power Sources 177 (2008) 131–136.
[39] Y. Wang, D.O. Northwood, J. Power Sources 165 (2007) 293–298.
[40] W.-S. Jeon, J.-G. Kim, Y.-J. Kim, J.-G. Han, Thin Solid Films 516 (2008) 3669–3672.
[41] P. Panjan, M. Cekada, M. Panjan, D. Kek-Merl, Vacuum 84 (2010) 209–214.
[42] M.F. Ashby, Materials Selection in Mechanical Design, 4th ed., Elsevier, Oxford, UK, 2010.
[43] B.K. Kakati, D. Sathiyamoorthy, A. Verma, Int. J. Hydrogen Energy 35 (2010) 4185–4194.
[44] R.A. Antunes, M.C.L. De Oliveira, G. Ett, Int. J. Hydrogen Energy 36 (2011) 12474–12485.
[45] A. Shanian, O. Savadogo, J. Power Sources 159 (2006) 1095–1104.
[46] R.V. Rao, Mater. Des. 29 (2008) 1949–1954.
[47] J. Zander, R. Sandström, Mater. Des. 32 (2011) 4866–4873.
[48] A. Thakker, J. Jarvis, M. Buggy, A. Sahed, Mater. Des. 29 (2008) 1973–1980.
[49] A. Jahan, F. Mustapha, M.Y. Ismail, S.M. Sapuan, M. Bahraminasab, Mater. Des. 32 (2011) 1215–1221.
[50] P. Chaterjee, V.M. Athawale, S. Chakraborty, Mater. Des. 32 (2011) 851–860.
[51] C.-C. Zhou, G.-F. Yin, X.-B. Hu, Mater. Des. 30 (2009) 1209–1215.
[52] A. Jahan, M.Y. Ismail, S.M. Sapuan, F. Mustapha, Mater. Des. 31 (2010) 696–705.
[53] A.I. Fernandez, M. Martínez, M. Segarra, I. Martorell, L.F. Cabeza, Sol. Energy Mater. Sol. Cells 94 (2010) 1723–1729.
[54] G.P. Reddy, N. Gupta, Mater. Des. 31 (2010) 113–117.
[55] O. Parate, N. Gupta, Mater. Des. 32 (2011) 1577–1581.
[56] A. Wanner, Mater. Des. 31 (2010) 2834–2839.
[57] Z. Bin, M. Bingchu, S. Chunhui, Y. Runzhang, J. Power Sources 161 (2006) 997–1001.
[58] www.emeigroup.com/images/pro3/pdf35/BMC_940.pdf (accessed 11.05.11).
[59] S. Chunhui, P. Mu, W. Qiong, Y. Runzhang, J. Power Sources 159 (2006) 1078–1083.
[60] S. Chunhui, P. Mu, H. Zhoufa, Y. Runzhang, J. Power Sources 166 (2007) 419–423.
[61] B.D. Cunningham, J. Huang, D.G. Baird, J. Power Sources 165 (2007) 764–773.
[62] S.R. Dhakate, R.B. Mathur, B.K. Kakati, T.L. Dhami, Int. J. Hydrogen Energy 32 (2007) 4537–4543.
[63] S.R. Dhakate, R.B. Mathur, S. Sharma, M. Borah, T.L. Dhami, Energy Fuels 23 (2009) 934–941.
[64] L. Du, S.C. Jana, J. Power Sources 172 (2007) 734–741.
[65] C. Du, P. Ming, M. Hou, J. Fu, Q. Shen, D. Liang, Y. Fu, X. Luo, Z. Shao, B. Yi, J. Power Sources 195 (2010) 794–800.
[66] S.I. Heo, J.C. Yun, K.S. Oh, K.S. Han, Adv. Compos. Mater. 15 (2006) 115–126.

[67] S.I. Heo, K.S. Oh, J.C. Yun, S.H. Jung, Y.C. Yang, K.S. Han, J. Power Sources 171 (2007) 396–403.
[68] J. Huang, D.G. Baird, J.E. McGrath, J. Power Sources 150 (2005) 110–119.
[69] C. Hui, L. Hong-Bo, Y. Li, L. Jian-xin, Y. Li, Int. J. Hydrogen Energy 35 (2010) 3105–3109.
[70] B.K. Kakati, D. Deka, Electrochim. Acta 52 (2007) 7330–7336.
[71] J.H. Lee, Y.K. Jang, C.E. Hong, N.H. Kim, P. Li, H.K. Lee, J. Power Sources 193 (2009) 523–529.
[72] S.-H. Liao, C.-H. Hung, C.-C.M. Ma, C.-Y. Yen, Y.-F. Lin, C.-C. Weng, J. Power Sources 176 (2008) 175–182.
[73] S.-H. Liao, C.-Y. Yen, C.-C. Weng, Y.-F. Lin, C.-C.M. Ma, C.-H. Yang, M.-C. Tsai, M.-Y. Yen, M.-C. Hsiao, S.-J. Lee, X.-F. Xie, Y.-H. Hsiao, J. Power Sources 185 (2008) 1225–1232.
[74] S.-H. Liao, M.-C. Hsiao, C.-Y. Yen, C.-C.M. Ma, S.-J. Lee, A. Su, M.-C. Tsai, M.-Y. Yen, L. Liu, J. Power Sources 195 (2010) 7808–7817.
[75] B. Luo, M. Hu, F. Li, G. Cao, Int. J. Hydrogen Energy 35 (2010) 2643–2647.
[76] P.H. Maheshwari, R.B. Mathur, T.L. Dhami, J. Power Sources 173 (2007) 394–403.
[77] R.B. Mathur, S.R. Dhakate, D.K. Gupta, T.L. Dhami, R.K. Aggarwal, J. Mater. Process. Technol. 203 (2008) 184–192.
[78] F. Mighri, M.A. Huneault, M.F. Champagne, Polym. Eng. Sci. 44 (2004) 1755–1765.
[79] http://www.biservice.lv/pdfi/Schunk_MoldedBipolarPlates-for-FuelCells.pdf (accessed 17.11.11).
[80] http://www.eisenhuth.de/pdf/SIGRACET_Datenblaetter.pdf (accessed 17.11.11).
[81] http://www.eisenhuth.de/pdf/SIGRACET_Datenblaetter.pdf (accessed 17.11.11).
[82] http://www.eisenhuth.de/pdf/SIGRACET_Datenblaetter.pdf (accessed 17.11.11).
[83] L.N. Song, M. Xiao, Y.Z. Meng, Combust. Sci. Technol. 66 (2006) 2156–2162.
[84] L.-G. Xia, A.-J. Li, W.-Q. Wang, Q. Yin, H. Lin, Y.-B. Zhao, J. Power Sources 178 (2008) 363–367.
[85] M. Xiao, Y. Lu, S.J. Wang, Y.F. Zhao, Y.Z. Meng, J. Power Sources 160 (2006) 165–174.
[86] T. Yang, P. Shi, J. Power Sources 175 (2008) 390–396.
[87] C.-Y. Yen, S.-H. Liao, Y.-F. Lin, C.-H. Hung, Y.-Y. Lin, C.-C.M. Ma, J. Power Sources 162 (2006) 309–315.
[88] Q. Yin, A.-J. Li, W.-Q. Wang, L.-G. Xia, Y.-M. Wang, J. Power Sources 165 (2007) 717–721.
[89] Q. Yin, K.-N. Sun, A.-J. Li, L. Shao, S.-M. Liu, C. Sun, J. Power Sources 175 (2008) 861–865.
[90] C.-Y. Bai, T.-M. Wen, K.-H. Hou, M.-D. Ger, J. Power Sources 195 (2010) 779–786.
[91] C.-Y. Bai, J.-L. Lee, T.-M. Wen, K.-H. Hou, M.-S. Wu, M.-D. Ger, Appl. Surf. Sci. 257 (2011) 3529–3537.
[92] J. Barranco, F. Barreras, A. Lozano, M. Maza, J. Power Sources 196 (2011) 4283–4289.
[93] M.P. Brady, H. Wang, B. Yang, J.A. Turner, M. Bordignon, R. Molins, M.A. Elhamid, L. Lipp, L.R. Walker, Int. J. Hydrogen Energy 32 (2007) 3778–3788.
[94] K. Feng, X. Cai, H. Sun, Z. Li, P.K. Chu, Diamond Relat. Mater. 19 (2010) 1354–1361.
[95] K. Feng, Z. Li, X. Cai, P.K. Chu, Mater. Chem. Phys. 126 (2011) 6–11.
[96] K. Feng, D.T.K. Kwok, D. Liu, Z. Li, X. Cai, P.K. Chu, J. Power Sources 195 (2010) 6798–6804.
[97] E. Fleury, J. Jayaraj, Y.C. Kim, H.K. Seok, K.Y. Kim, K.B. Kim, J. Power Sources 159 (2006) 34–37.
[98] Y. Fu, M. Hou, G. Lin, J. Hou, Z. Shao, B. Yi, J. Power Sources 176 (2008) 282–286.
[99] T. Fukutsuka, T. Yamaguchi, S.-I. Miyano, Y. Matsuo, Y. Sugie, Z. Ogumi, J. Power Sources 174 (2007) 199–205.
[100] W.-Y. Ho, H.-J. Pan, C.-L. Chang, D.-Y. Wang, J.J. Hwang, Surf. Coat. Technol. 202 (2007) 1297–1301.
[101] J. Jayaraj, Y.C. Kim, H.K. Seok, K.B. Kim, E. Fleury, Mater. Sci. Eng. A 449–451 (2007) 30–33.
[102] K.M. Kim, K.Y. Kim, J. Power Sources 173 (2007) 917–924.
[103] K.M. Kim, J.H. Park, J.H. Kim, K.Y. Kim, Int. J. Hydrogen Energy 36 (2011) 9926–9935.
[104] M. Kumagai, S.-T. Myung, S. Kuwata, R. Asaishi, H. Yashiro, Electrochim. Acta 53 (2008) 4205–4212.
[105] O. Lavigne, C. Alemany-Dumont, B. Normand, P. Delichère, A. Descamps, Surf. Coat. Technol. 205 (2010) 1870–1877.
[106] Y.-B. Lee, D.-S. Lim, Curr. Appl. Phys. 10 (2010) S18–S21.
[107] Y.-B. Lee, C.-H. Lee, D.-S. Lim, Int. J. Hydrogen Energy 34 (2009) 9781–9787.
[108] S.-T. Myung, M. Kumagai, R. Asaishi, Y.-K. Sun, H. Yashiro, Electrochem. Commun. 10 (2008) 480–484.
[109] D.-G. Nam, H.-C. Lee, J. Power Sources 170 (2007) 268–274.
[110] A. Pozio, F. Zaza, A. Masci, R.F. Silva, J. Power Sources 179 (2008) 631–639.
[111] R.F. Silva, D. Franchi, A. Leone, L. Pilloni, A. Masci, A. Pozio, Electrochim. Acta 51 (2006) 3592–3598.
[112] R. Tian, J. Sun, L. Wang, Int. J. Hydrogen Energy 31 (2006) 1874–1878.
[113] R. Tian, J. Power Sources 196 (2011) 1258–1263.
[114] H. Wang, M.P. Brady, G. Teeter, J.A. Turner, J. Power Sources 138 (2004) 86–93.
[115] H. Wang, M.P. Brady, K.L. More, H.M. Meyer III, J.A. Turner, J. Power Sources 138 (2007) 79–85.
[116] H. Wang, J.A. Turner, J. Power Sources 128 (2004) 193–200.
[117] H. Wang, J.A. Turner, X. Li, R. Bhattacharya, J. Power Sources 171 (2007) 567–574.
[118] K.S. Weil, G. Xia, Z.G. Yang, J.Y. Kim, Int. J. Hydrogen Energy 32 (2007) 3724–3733.
[119] T.-M. Wen, K.-H. Hou, C.-Y. Bai, M.-D. Ger, P.-H. Chien, S.-J. Lee, Curr. Sci. 52 (2010) 3599–3608.
[120] B. Wu, G. Lin, Y. Fu, M. Hou, B. Yi, Int. J. Hydrogen Energy 35 (2010) 13255–13261.
[121] B. Yang, M.P. Brady, H. Wang, J.A. Turner, K.L. More, D.J. Young, P.F. Tortorelli, E.A. Payzant, L.R. Walker, J. Power Sources 174 (2007) 228–236.
[122] Y. Yang, L.-J. Guo, H. Liu, Int. J. Hydrogen Energy 36 (2011) 1654–1663.
[123] Y. Yang, L. Guo, H. Liu, J. Power Sources 196 (2011) 5503–5510.
[124] W. Yoon, X. Huang, P. Fazzino, K.L. Reifsnider, M.A. Akkaoui, J. Power Sources 179 (2008) 265–273.
[125] R. Tian, J. Sun, Int. J. Hydrogen Energy 36 (2011) 6788–6794.
[126] M. Zhang, B. Wu, G. Lin, Z. Shao, M. Hou, B. Yi, J. Power Sources 196 (2011) 3249–3254.
[127] H. Zhang, G. Lin, M. Hou, L. Hu, Z. Han, Y. Fu, Z. Shao, B. Yi, J. Power Sources 198 (2012) 176–181.
[128] L. Wang, J. Sun, J. Sun, Y. Lv, S. Li, S. Ji, Z. Wen, J. Power Sources 198 (2012) 195–200.
[129] W. Jin, K. Feng, Z. Li, X. Cai, L. Yu, D. Zhou, J. Power Sources 196 (2011) 10032–10037.
[130] L. Wang, D.O. Northwood, X. Nie, J. Housden, E. Spain, A. Leyland, A. Matthews, J. Power Sources 195 (2010) 3814–3821.
[131] K. Feng, T. Hu, X. Cai, Z. Li, P.K. Chu, J. Power Sources 199 (2012) 207–213.
[132] K. Feng, Y. Shen, J. Mai, D. Liu, X. Cai, J. Power Sources 182 (2008) 145–152.
[133] R.A. Antunes, M.C.L. De Oliveira, Crit. Rev. Biomed. Eng. 37 (2009) 425–460.